Hindawi
International Journal of Polymer Science
Volume 2021, Article ID 9919982, 8 pages
https://doi.org/10.1155/2021/9919982

Research Article

Treatment and Nursing Values of Cd(II) Complex with Photocatalytic Activity on Bacterial Infection by Inhibiting the Gram-Positive Bacteria Growth

Jing Peng[1], **Quan-Zhen Tang**[1], **Jian Lu**[1], **Yan Hu**[2] and **Jiao Ni**[2]

[1]*Department of Infectious Diseases, Shenzhen University General Hospital, Shenzhen Guangdong, China*
[2]*Department of Medicine, People's Hospital, Zhuji, Zhejiang, China*

Correspondence should be addressed to Jian Lu; owfctjdvaetk38@163.com

Received 23 March 2021; Revised 22 July 2021; Accepted 24 August 2021; Published 25 September 2021

Academic Editor: Atsushi Sudo

Presented here is a trinuclear cluster-based Cd(II) compound, namely, $\{[(CH_3)_2NH_2][Cd_6K(bdc)_6(btz)_3(H_2O)_6]\}_n$ (**1** H_2bdc = terephthalic acid, Hbtz = 1H-benzotriazole), has been solvothermally prepared and structurally determined by the single crystal X-ray diffraction analysis, elemental analysis, powder X-ray diffraction analysis, and thermogravimetric analysis. Notably, compound **1** shows excellent photocatalytic activity for degradation of MV irradiated by UV light. In addition to this, the biological activity of the new compound on bacterial infection was evaluated, and the corresponding mechanism was also studied. The ELISA assay was used to evaluate the TNF-α and IL-1β released into plasma after compound treatment. Then, the relative expression levels of the bacterial survival gene were measured with real-time RT-PCR.

1. Introduction

A hospital is a place with intensive patients, and the hospital environment is most likely to be contaminated by pathogenic microorganisms, which provides external conditions for the spread of diseases and promotes the occurrence of nosocomial infections [1]. Nosocomial infections bring serious harm to society and individuals. In the past two decades, the incidence of methicillin-resistant Staphylococcus aureus infection in hospitals has been increasing year by year, and it can cause outbreaks of nosocomial infections, with a mortality rate as high as 50% [2, 3]. The Cd-based coordination complex has various of bioactivity, such as anticancer and anti-inflammatory activity [4]. Thus, we further evaluate the antibacterial activity of the new compound.

Metal-organic frameworks (MOFs) with charming topological architectures, high surface areas and porosities, and tunable pore structures can find huge potential applications in luminescent sensors, ion exchange, heterogeneous catalysis, gas storage, separation, etc. [5–9]. Currently, MOF-based photocatalysts are of current research interest owing to their high catalytic efficiencies and eco-friendly economic for the photocatalytic degradation of organic dye contaminants existing in the wastewater discharge [10–13]. Therefore, how to rationally design and synthesize MOFs that can effectively adsorb UV/UV-Vis/visible light has become a puzzle to synthetic chemists. Such property of MOFs for the absorption of adsorb UV/UV-Vis/visible light is intimately related with the organic ligands with appropriate functional group and rigidity as well as the symmetry. According to the reports, mixed-ligand strategy is considered to be one of the most effective methods for the construction of target MOFs that can serve as photocatalysts for the water purification [14]. For this method, the organic building blocks are the combination of two function-different ligands that also termed as acid-base mixed-ligand system. In the past few years, the combination of N-donor ligand and polycarboxylate ligand is often used as the acid-base mixed-ligand system for the construction of MOFs with promising potential functions [15–18].

Based on the aforementioned considerations, in this work, we selected 1H-benzotriazole and terephthalic acid as the organic building skeletons in that the synergistic action of 1H-benzotriazole and terephthalic acid with metal

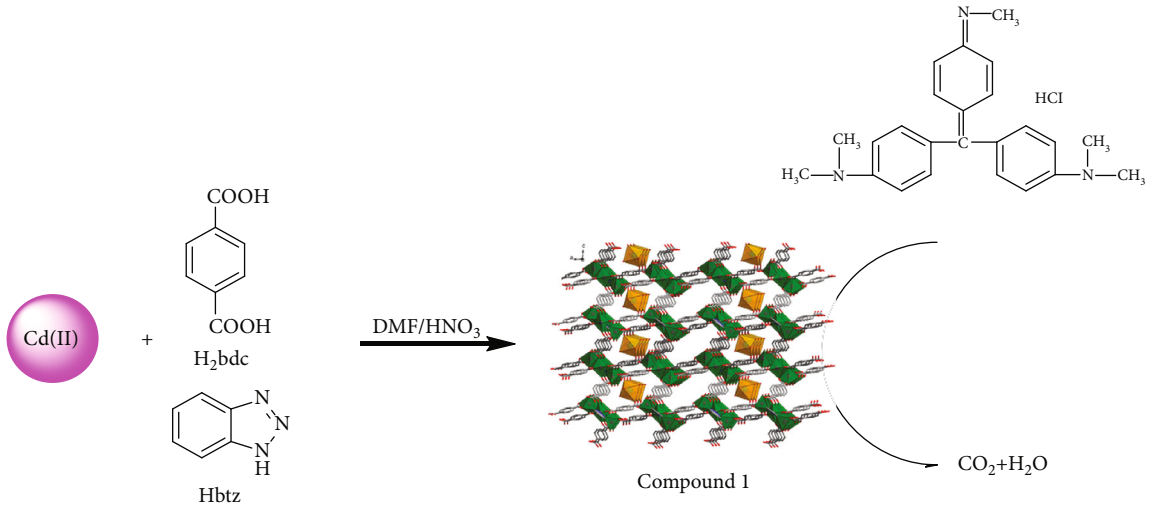

Scheme 1: The synthetic route for **1** in this work.

ions may result in polynuclear cluster-based building subunits [19]. Under the solvothermal conditions, the self-assembly of 1H-benzotriazole and terephthalic acid as well as Cd(II) ions successfully afforded a new trinuclear $[Cd_3(btz)(COO)_4]$ cluster-based compound, namely, $\{[(CH_3)_2NH_2][Cd_6K(bdc)_6(btz)_3(H_2O)_6]\}_n$ (**1** H_2bdc = terephthalic acid, Hbtz = 1H-benzotriazole, Scheme 1). X-ray structural analysis revealed that compound **1** has a 3D framework with 6-connected *pcu* topology. In the following, the synthetic method, crystal structure, and photocatalytic property of **1** will be described in detail. In the biological section, the application values of the compound on *Staphylococcus aureus* bacterial infection were assessed, followed by the mechanism exploration. The results of the ELISA assay indicated that the compound could significantly reduce the content of TNF-α and IL-1β released into plasma. Besides, the data of real-time RT-PCR indicated that the bacterial survival gene expression was also exhibited by the new compound.

2. Experimental

2.1. Materials and Equipment. The starting chemical regents were purchased commercially and used without further purification. C, H, and N elemental were determined by a Perkin-Elmer 240 elemental analyzer. Power X-ray diffraction was recorded with a Bruker AXS D8 advanced automated diffractometer with Cu/*K*a radiation ($\lambda = 1.5406$ Å) at room temperature. Thermogravimetric analysis was carried out on a NetzschSTA499C integration thermal analyzer under N_2 atmosphere from 30 to 800°C at a heating rate of 10°C/min. Single crystal X-ray diffraction analysis was performed using a computer-controlled Oxford Xcalibur E diffractometer with graphite-monochromated Mo/Kα radiation ($\lambda = 0.71073$ Å).

2.2. Synthesis of $\{[(CH_3)_2NH_2][Cd_6K(bdc)_6(btz)_3(H_2O)_6]\}_n$. A mixture of $Cd(NO_3)_2{\cdot}4H_2O$ (0.2 mmol, 0.062 g), KNO_3 (0.05 mmol), H_2bdc (0.2 mmol, 0.036 g), Hbtz (0.2 mmol, 0.024), DMF (3 mL), and concentrated nitric acid (1 drops) was placed in a 20 mL small glass vial, which was heated at 110°C for 36 h and then cooled to room temperature at a rate of 2°C/min. Colorless block crystals yield in 35% based on $Cd(NO_3)_2{\cdot}4H_2O$. Anal. Calcd. (%) for **1** $C_{62}H_{52}Cd_6KN_7O_{30}$ (2088.65) are as follows: C, 35.62; H, 2.49; and N, 4.69%. Found (%) are as follows: C, 35.64; H, 2.47; and N, 4.71%.

2.3. Structure Determination. The single crystal structure of **1** was solved using the dual direct methods and refined by the full-matrix least squares technique based on F^2 using the SHELXL-2014 program [20]. All the H atoms were generated at their ideal locations, and all nonhydrogen atoms in the structure were refined anistropically. The detailed crystallographic data and structural refinements of **1** are summarized in Table 1. Selected bond lengths (Å) and angles (°) of **1** are listed in Table S1.

2.4. Photocatalytic Experiments. 50 mg powder samples of **1** were added into 100 mL of 10 mg·L^{-1} MV aqueous solution. Then, the suspension was magnetically stirred in the dark for about 2 h to establish the adsorption-desorption equilibrium. After that, the photocatalytic experiment was carried out using XPA-7 type photochemical reactor equipped with a 125 W Hg (365 nm) lamp. 5 mL reaction mixture was taken out every 15 minutes and further separated through centrifugation. Then, subsequently, the characteristic electronic absorption band of MV was measured using UV-Vis spectrophotometer. The obtained solution was analyzed by the UV-Vis absorption spectrometer.

2.5. ELISA Assay. The ELISA detection kit was conducted in this present research to measure the content of TNF-α and IL-1β released into plasma after compound treatment. This conduction was accomplished fully on the basis of instructions with a little modification. In short, 50 BALB/c mice used in the study were purchased from the Zhongshan University Experimental Animal Center (ZSXK 2020-0017). The 10^8 CFU *Staphylococcus aureus* bacterial cells were injected

Table 1: Crystal data and structure refinements for compound **1**.

Formula	$C_{62}H_{52}Cd_6KN_7O_{30}$
Fw	2088.65
Crystal system	Monoclinic
Space group	$P2_1/c$
a (Å)	25.7641(11)
b (Å)	11.2486(5)
c (Å)	18.8369(12)
A (°)	90.00
β (°)	92.937(4)
γ (°)	90.00
V (Å^3)	5452.0(5)
Z	4
Density (calculated)	1.244
Abs. coeff. (mm^{-1})	1.245
Total reflections	24355
Unique reflections	12326
Goodness of fit on F^2	0.975
Final R indices $\left[I > 2\text{sigma}\left(I^2\right)\right]$	$R = 0.0735$, $wR_2 = 0.2094$
R (all data)	$R = 0.1046$, $wR_2 = 0.2372$
CCDC	2055973

into the mice to induce the *Staphylococcus aureus* bacterial infection model. Next, the compound was given for treatment at 1 mg/kg, 2 mg/kg, and 5 mg/kg concentration, respectively. In the last, the plasma of different animal was harvested and the TNF-α and IL-1β content released into plasma was measured via the ELISA detection kit.

2.6. Real-Time RT-PCR. After the infection model construction and the compound treatment, the real-time RT-PCR was further conducted and the *Staphylococcus aureus* bacterial survival gene relative expression levels were determined. This conduction was finished strictly in accordance with the instructions with minor change. In short, the 10^8 CFU *Staphylococcus aureus* bacterial cells were collected and seeded into 6-well cell culture plates; next, the compound was given for treatment at the concentration of 10 ng/mL, 20 ng/mL, and 50 ng/mL. Subsequently, the bacterial cells were collected, and the entire RNA in the bacterial cells was extracted via the reagent of TRIZOL. After measuring the entire RNA concentration, this concentration was then reverse transcripted into the cDNA. In the end, the *Staphylococcus aureus* bacterial survival gene relative expression levels were detected by real-time RT-PCR, with *gapdh* used as the internal control gene.

3. Results and Discussions

3.1. Crystal Structure. X-ray diffraction analysis for **1** revealed that it crystallizes in the monoclinic $P2_1/c$ space group and displays a 3D framework with the asymmetric unit including three Cd(II) ions, a half K^+ ion, three bdc^{2-} ligands, one btz^- ligand, three coordinated water molecules, and a half disordered $NH_2(CH_3)^+$ cation that has not been well modeled. As shown in Figure 1(a), Cd1 displays a pentagonal bipyramidal geometry with four carboxylate oxygen atoms and one nitrogen atom in the equatorial plane and one carboxylate oxygen atom and one terminal water molecule in the axial position. Cd2 and Cd3 are six-coordinated with distorted octahedral coordination geometries. For Cd2, the distorted octahedron is defined by three carboxylate oxygen atoms and one nitrogen atom in the equatorial plane and another carboxylate oxygen atom and one water ligand in the axial sites. For Cd3, the distorted octahedron is defined by three carboxylate oxygen atoms and one nitrogen atom in the equatorial plane and another two carboxylate oxygen atoms in the axial sites. The K1 ion is six-coordinated by four water ligands in the equatorial plane and two carboxylate oxygen atoms in the axial sites, affording an octahedron. The Cd-O, Cd-N, and K-O distances are in the range of 2.244(5)-2.611(7) Å, 2.263(6)-2.279(6) Å, and 2.239(13)-2.828(9) Å, respectively, which are in the normal range based on previously related Cd-based MOFs [21]. The bdc^{2-} ligand displays two different coordination modes that are shown in Fig. S1. Crystallographically independent three Cd(II) ions are bridged by one btz^- ligand and four carboxylate groups, forming a trinuclear $[Cd_3(btz)(COO)_4]$ cluster with the average Cd$\cdots$Cd distance of 3.65 Å (Figure 2(b)). Such trinuclear cluster-based building subunits are further bridged together by the pdc^{2-} ligands and the $[KO_6]$ octahedrons, leading to the formation of a 3D framework (Figure 2(c)). In this 3D framework, each trinuclear cluster is bonded to six neighboring identical ones *via* the six pdc^{2-} ligands. Topologically speaking, this 3D framework of **1** can be reduced into a 6-connected *pcu* topological network with the point symbol of $\{4^{12}\cdot6^3\}$ by viewing trinuclear $[Cd_3(btz)(COO)_4]$ clusters as 6-connected node and pdc^{2-} ligands as linear connectors (Figure 2(d)).

3.2. Powder X-Ray Diffraction (PXRD) Pattern and Thermogravimetric Analysis (TGA). Via the result of the PXRD experiment shown in Figure 1(a), it can be observed that the experiment pattern based on the as-synthesized bulk samples shows a good match with that of the simulated pattern based on the single crystal diffraction data, which is indicative of good phase purity. In addition, we also investigated the thermal behavior of **1** under nitrogen atmosphere ranging from 30 to 800°C. As shown in Figure 1(b), the release of the coordinated water molecules from the skeleton of **1** occurred in temperature range of 96-125°C with a weight loss of 5.19% (Calcd: 5.17%), and further, the solvent-free compound shows a good stability until 302°C. Finally, the significant weight loss from 302 to 439°C corresponds to the decomposition of the organic ligands.

3.3. Photocatalytic Property. According to the reports of Cd(II)-based MOFs, we found that most of them show excellent photocatalytic activities for the degradation of organic dyes upon exposure to UV or visible light [22, 23]. Herein, the photocatalytic property of **1** was estimated by the selection of methyl violet (MV) as a model contaminant. The characteristic absorption peak at 580 nm for MV was

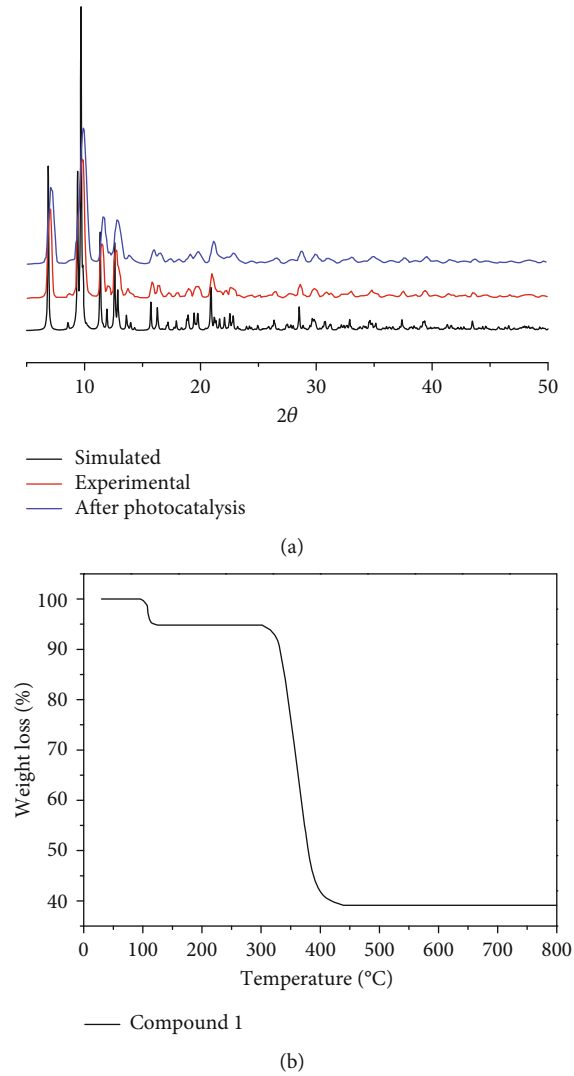

Figure 1: (a) Powder X-ray diffraction patterns for **1**. (b) The TGA curve for **1**.

selected to monitor the photocatalytic process. The control experiment without 1 as photocatalyst was also conducted under the same conditions. In the presence of **1**, the absorption intensities at 580 nm weakened gradually with the time increase of the UV light irradiation (Figure 3(a)). According to the plots of C_t/C_0 versus irradiation time (t) (Figure 3(b)), it can be calculated that about 90.6% MV in solution underwent photodegradation in the presence of **1**, and only 13.3% MV in solution was photodegraded in absence of **1**, indicating the good photocatalytic activity of **1** for the degradation of MV under UV light irradiation. Such photocatalytic reaction of MV is in line with the first-order kinetic equation of $\ln(C_0/C_t) = -kt + b$ (C_0 and C_t represent the initial concentration of MV solution and the concentration of MV solution at the irradiation time of t, k is the rate constant, and b is a constant), and the rate constant of k obtained from the linear fitting of $\ln(C_t/C_0)$ versus irradiation time (t) is 0.03273 min^{-1} (Figure 2(c)). The PXRD patterns before and after the photocatalytic reaction show no significant difference, demonstrating the good structural stability of **1** during the photocatalytic process (Figure 1(a)). Furthermore, we also performed four successive experiments at the same conditions, and the degradation efficiency of MV remains above 90% after the fourth experiment (Figure 3(d)), indicating that the photocatalytic activity of **1** is stable for the degradation of MV.

3.4. Significantly Reduced the TNF-α and IL-1β Releasing into Plasma after Treating via Compound. After the synthesis of the new compound with novel structure, its biological activity was assessed and the mechanism was explored as well. Thus, the ELISA detection kit was carried out in this experiment for the detection of the inhibitory activity of the compound on the IL-1β and TNF-α level released into plasma. As the results illustrated in Figure 4, we can see that model group has a significantly enhanced IL-1β level and the TNF-α level released into plasma, in contrast to control group, with $P < 0.005$. However, after the treatment of the new compound, the IL-1β and the TNF-α content released into plasma was significantly inhibited. The

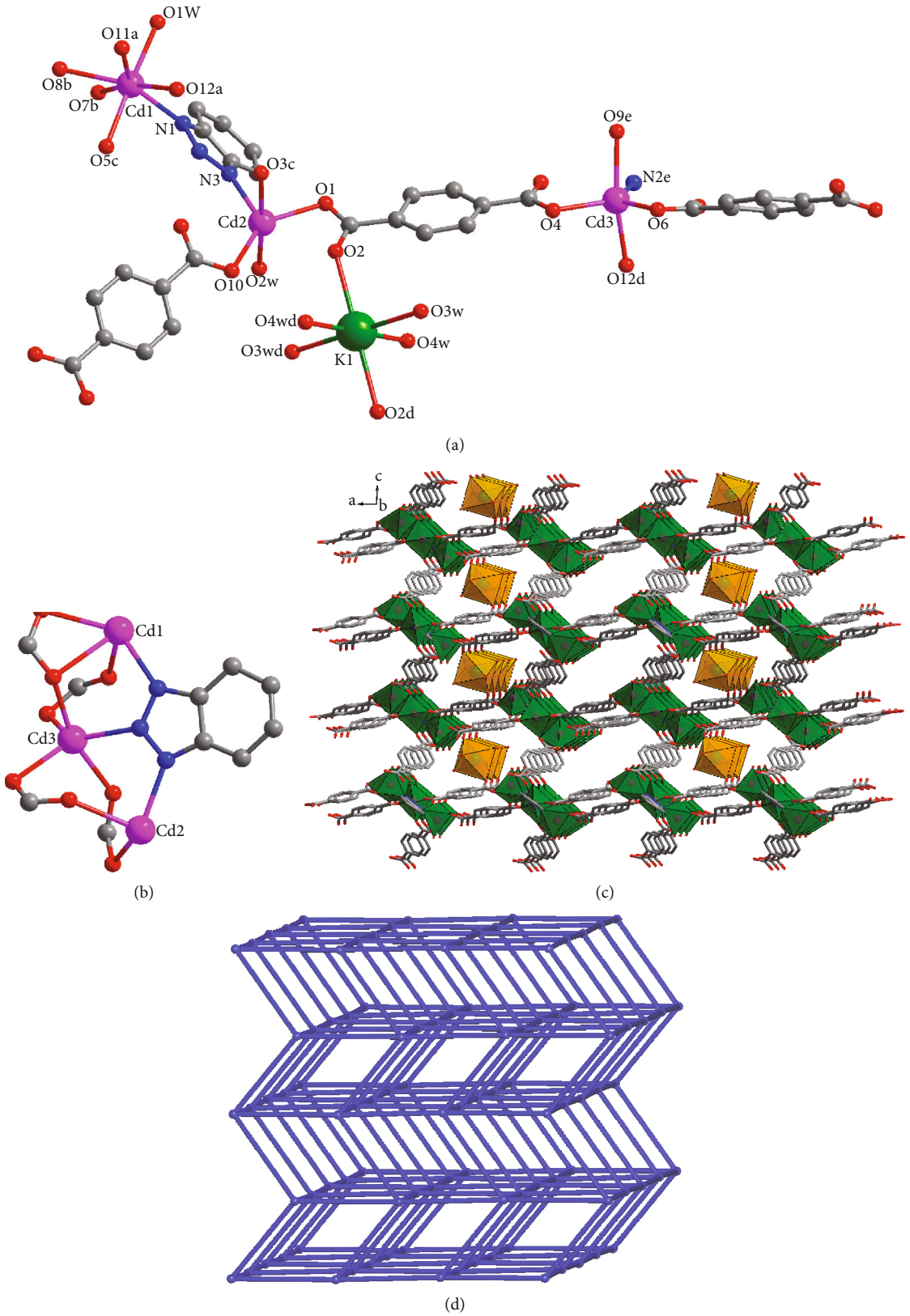

FIGURE 2: (a) View of the environments of Cd(II) ions in **1**. (b) Trinuclear $[Cd_3(btz)(COO)_4]$ cluster-based building subunit for **1**. (c) The 3D framework of **1**. (d) Schematic representation of the 6-connected *pcu* topological network for **1**.

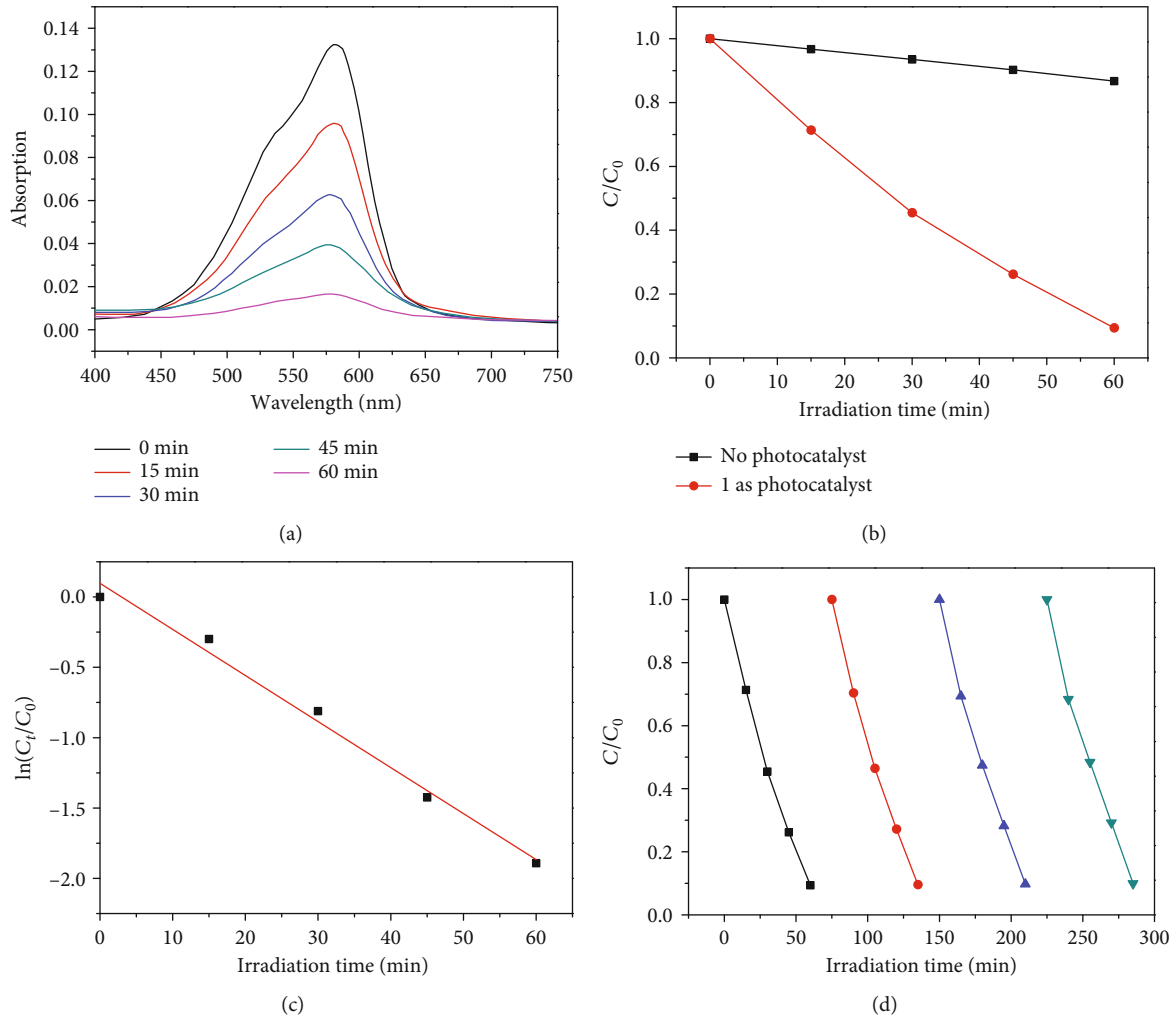

Figure 3: (a) The UV-Vis absorption spectra of MV in the presence of **1** with the increase of irradiation time. (b) Percentage of MV remaining in the solution monitored with time. (c) Photocatalytic degradation kinetic of **1** for MV using first-order kinetic equation of $\ln(C_t/C_0) = -\kappa t + b$. (d) Cycling runs for the photocatalytic degradation of MV under UV light irradiation.

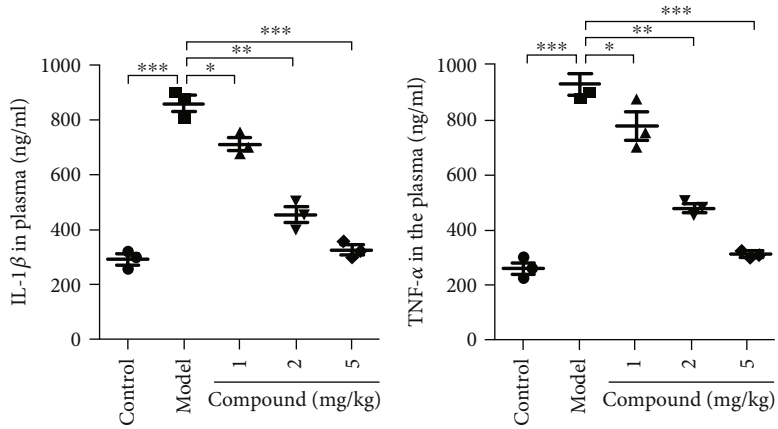

Figure 4: Compound significantly reduces the releasing of the IL-1β and TNF-α into the plasma. 10^8 CFU *Staphylococcus aureus* was injected into the animal to induce the bacterial infection animal model; then, the compound was used for treatment at the concentration of 1, 2, and 5 mg/kg. After the treatment, the plasma was harvested and the IL-1β and TNF-α content released into plasma was measured through the ELISA detection kit.

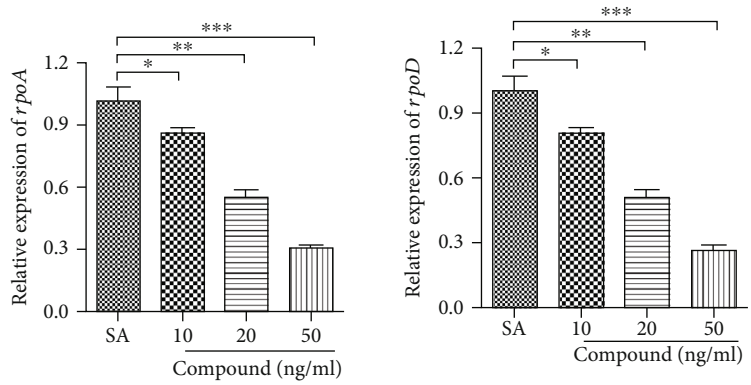

Figure 5: Compound obviously inhibited the relative expression of the *Staphylococcus aureus* bacterial survival gene. *Staphylococcus aureus* bacterial cells were incubated with serial different concentration of the compound. Then, the real-time RT-PCR was conducted, and the real-time RT-PCR was performed to determine the relative expression of the *Staphylococcus aureus* bacterial survival gene.

inhibition of the new compound showed a dose-dependent manner.

3.5. Significantly Inhibited the Staphylococcus aureus Bacterial Survival Gene Relative Expression after Treated with the Compound. In the above experiment, we have confirmed that this compound has excellent inhibitory activity on the releasing of IL-1β and TNF-α into the plasma in a dose-dependent manner. Furthermore, the compound's inhibitory activity against the *Staphylococcus aureus* bacterial survival gene relative expression was further determined with real-time RT-PCR. The results in Figure 5 inhibited that compared with the control group, this complex could evidently downregulate the *Staphylococcus aureus* bacterial survival gene relative expression. This inhibition suggested the dose-dependent manner.

4. Conclusions

In conclusion, a new Cd(II) compound has been solvothermally synthesized based on the organic ligands of H_2bdc and Hbtz. X-ray structural analysis revealed that it features a 3D framework with trinuclear $[Cd_3(btz)(COO)_4]$ cluster-based subunits and can be simplified into a 6-connected *pcu* topological network by looking the trinuclear clusters as 6-connected nodes and the bdc^{2-} ligands as the linear connectors. Under UV light irradiation, this compound exhibits good photocatalytic activity for the degradation of MV, and after four cycles, the degradation efficiency of MV remains above 90%. The results of the ELISA assay indicated that the compound could significantly reduce the content of TNF-α and IL-1β released into plasma. Besides, the data of real-time RT-PCR indicated that the bacterial survival gene expression was also exhibited by the new compound. In the end, it can be concluded that this compound possesses potential to be an outstanding candidate for the *Staphylococcus aureus* bacterial infection treatment by inhibiting the IL-1β and TNF-α releasing.

Data Availability

The table showing the bond lengths and angles for complex 1 (Table S1) could be found in the supporting information file.

Conflicts of Interest

The authors declare that there is no conflict of interest regarding the publication of this paper.

Acknowledgments

This work was supported by grants from the Natural Science Foundation of Shenzhen University General Hospital, Shenzhen University Clinical Medical Academy (SUGH2018QD047) and Shenzhen Basic Research Key projects, Shenzhen Science and Technology Innovation Commission (JCYJ2015 0402111430617).

Supplementary Materials

Table S1: selected bond lengths (Å) and angles (°) for **1**. Fig. S1: the coordination modes of pdc^{2-} ligand in **1**. *(Supplementary Materials)*

References

[1] S. H. Nasr, J. Radhakrishnan, and V. D. D'Agati, "Bacterial infection-related glomerulonephritis in adults," *Kidney International*, vol. 83, no. 5, pp. 792–803, 2013.

[2] Y. Xiao and W. Cai, "Autophagy and bacterial infection," *Advances in Experimental Medicine and Biology*, vol. 1207, pp. 413–423, 2020.

[3] C. Zhu, Y. Wang, C. Cai, and Q. Cai, "Bacterial infection and associated cancers," *Advances in Experimental Medicine and Biology*, vol. 1018, pp. 181–191, 2017.

[4] Y. Hu and J. Ni, "A new trinuclear cluster-based Cd(II) compound: photocatalytic property and nursing application values on the bacterial infection," *Designed Monomers and Polymers*, vol. 24, no. 1, pp. 175–183, 2021.

[5] L. Fan, F. Wang, D. Zhao et al., "Two cadmium(II) coordination polymers as multi-functional luminescent sensors for the detection of Cr(VI) anions, dichloronitroaniline pesticide, and nitrofuran antibiotic in aqueous media," *Spectrochimica Acta Part A: Molecular and Biomolecular Spectroscopy*, vol. 239, p. 118467, 2020.

[6] L. Fan, D. Zhao, B. Li et al., "An exceptionally stable luminescent cadmium(ii) metal–organic framework as a dual-functional chemosensor for detecting Cr(vi) anions and nitro-containing antibiotics in aqueous media," *CrystEngComm*, vol. 23, no. 5, pp. 1218–1225, 2021.

[7] L. Fan, F. Wang, D. Zhao et al., "A self-penetrating and chemically stable zinc (ii)-organic framework as multi-responsive chemo-sensor to detect pesticide and antibiotics in water," *Applied Organometallic Chemistry*, vol. 34, pp. 1218–1225, 2020.

[8] J. X. Li, Z. X. Du, L. Y. Xiong, L. L. Fu, and W. B. Bo, "Supramolecular isomerism in two nickel(II) coordination polymers constructed with the flexible 2-carboxyphenoxyacetate linker: syntheses, structure analyses and magnetic properties," *Journal of Solid State Chemistry*, vol. 293, p. 121799, 2021.

[9] J. X. Li, Z. X. Du, L. L. Zhang, D. L. Liu, and Q. Y. Pan, "Doubly mononuclear cocrystal and oxalato-bridged binuclear copper compounds containing flexible 2-((3,5,6-trichloropyridin-2-yl)oxy)acetate tectons: synthesis, crystal analysis and magnetic properties," *Inorganica Chimica Acta*, vol. 512, p. 119890, 2020.

[10] X. Feng, Y. Q. Feng, L. Liu, L. Y. Wang, H. L. Song, and S. W. Ng, "A series of Zn-4f heterometallic coordination polymers and a zinc complex containing a flexible mixed donor dicarboxylate ligand," *Dalton Transactions*, vol. 42, no. 21, pp. 7741–7754, 2013.

[11] X. Feng, N. Guo, R. F. Li et al., "A facile route for tuning emission and magnetic properties by controlling lanthanide ions in coordination polymers incorporating mixed aromatic carboxylate ligands," *Journal of Solid State Chemistry*, vol. 268, pp. 22–29, 2018.

[12] M. L. Hu, M. Y. Masoomi, and A. Morsali, "Template strategies with MOFs," *Coordination Chemistry Reviews*, vol. 387, pp. 415–435, 2019.

[13] M. L. Hu, V. Safarifard, E. Doustkhah et al., "Taking organic reactions over metal-organic frameworks as heterogeneous catalysis," *Microporous and Mesoporous Materials*, vol. 256, pp. 111–127, 2018.

[14] M. L. Hu, M. Abbasi-Azad, B. Habibi et al., "Electrochemical applications of ferrocene-based coordination polymers," *ChemPlusChem*, vol. 85, no. 11, pp. 2397–2418, 2020.

[15] H. Xu, H. Du, L. Kang, Q. Cheng, D. Feng, and S. Xia, "Constructing straight pores and improving mechanical properties of ganguebased porous ceramics," *Journal of Renewable Materials*, vol. 9, no. 12, pp. 2129–2141, 2021.

[16] C. Duan, Y. Yu, J. Li et al., "Recent advances in the synthesis of monolithic metal-organic frameworks," *Science China Materials*, vol. 64, no. 6, pp. 1305–1319, 2021.

[17] H. Zhang, J. H. Huo, J. Q. Li, F. Li, C. X. Duan, and H. X. Xi, "Hierarchically porous metal-organic frameworks with single-crystal structures and their enhanced catalytic properties," *CrystEngComm*, vol. 20, no. 38, pp. 5754–5759, 2018.

[18] D. Zhang, C. Bi, Z. Zong, and Y. Fan, "Three different Co(II) metal-organic frameworks based on 4,4′-Bis(imidazolyl)diphenyl ether: syntheses, crystal structure and photocatalytic properties," *Journal of Inorganic and Organometallic Polymers and Materials*, vol. 30, no. 12, pp. 5148–5156, 2020.

[19] Y. Y. Qin, J. Zhang, Z. J. Li, L. Zhang, X. Y. Cao, and Y. G. Yao, "Organically templated metal–organic framework with 2-fold interpenetrated {33.59.63}-lcy net," *Chemical Communications*, vol. 22, pp. 2532–2534, 2008.

[20] G. M. Sheldrick, "Crystal structure refinement withSHELXL," *Acta Crystallographica Section C*, vol. 71, no. 1, pp. 3–8, 2015.

[21] Y. Dong and G. Z. Xing, "Two new cadmium(II) compounds based on distinct second building subunits: solvothermal syntheses, crystal structures, and luminescent properties," *Zeitschrift für Anorganische und Allgemeine Chemie*, vol. 641, no. 10, pp. 1679–1683, 2015.

[22] X. J. Wei, D. Liu, Y. H. Li, and G. H. Cui, "New 2D and 3D Cd(II) coordination polymers from aromatic dicarboxylate and 1,3-bis(5,6-dimethylbenzimidazol-1-yl)-2-propanol ligands: syntheses, structures, photocatalytic, and luminescence sensing properties," *Journal of Solid State Chemistry*, vol. 272, pp. 138–147, 2019.

[23] W. C. Kang, Z. C. Hao, C. Han, and G. Y. J. Dong, "Multicomponent self-assembly of two Cd(II)-based coordination polymers: synthesis, structures and photocatalytic properties," *Journal of Inorganic and Organometallic Polymers and Materials*, vol. 30, no. 5, pp. 1877–1885, 2020.